Available online at www.sciencedirect.com
ScienceDirect
Ceramics International 36 (2010) 1311–1317
CERAMICS INTERNATIONAL
www.elsevier.com/locate/ceramint

Electrical and magnetic properties of magnesium-substituted lithium ferrite

Yen-Pei Fu [a,*], Shao-Hua Hu [b]

[a] Department of Materials Science and Engineering, National Dong-Hwa University, Shou-Feng, Hualien 974, Taiwan
[b] Department of Environmental Resources Management, Dahan Institute of Technology, Sincheng, Hualien 971, Taiwan

Received 6 October 2009; received in revised form 30 November 2009; accepted 29 December 2009
Available online 29 January 2010

Abstract

Magnesium-substituted lithium ferrite of different composition ($Li_{0.5}Fe_{2.5-x}Mg_xO_{4-\delta}$) were prepared for $x = 0.0$–1.0 by conventional ceramic technique. The crystal structure characterization and morphology were investigated by X-ray diffraction (XRD), scanning electron microscopy (SEM). Initial permeability and quality factor were measured in the frequency range of 1 kHz to 100 MHz. The permeability decreased gradually from μ ($f = 10$ MHz) = 34.0 for $Li_{0.5}Fe_{2.5}O_4$ to μ ($f = 10$ MHz) = 11.5 for $Li_{0.5}Fe_{1.5}Mg_{1.0}O_4$. Electrical conductivity measurements were carried in the range of 250–700 °C in air. The maximum electrical conductivity, $\sigma_{700\ ^\circ C} = 0.1274$ S/cm has been found to be for $Li_{0.5}Fe_{2.5}O_4$ specimen. With increasing Mg-substituted content, the decreased in the electrical conductivity.

Keywords: A. Powders: solid state reaction; C. Electrical properties; C. Magnetic properties; D. Spinels; E. Soft magnets

1. Introduction

Spinel ferrites have potential applications in electrical components such as memory devices and microwave devices over a wide range of frequency due to their high resistivity and loss behavior [1]. The family of substituted lithium ferrites have attracted the attention of scientists for a long time and have been developed as a replacement for yttrium iron garnet (YIG) owing to their low cost [2]. Lithium ferrites are important components of microwave devices such as isolators, circulars, gyrators, and phase shifters and memory cores owing to their high Curie temperature, high saturation magnetization, and hysteresis loop properties, which offer performance advantage over other spinel structures [3–6]. Since the number of ferric ions on A and B sites is unequal in lithium ferrite, the calculated magnetic moment is not just that of lithium ions, but is given by the difference in the magnetic moment of ions on A and B sites. Consequently, lithium ferrite possesses a higher Curie temperature than other spinel ferrites [7]. $Li_{0.5}Fe_{2.5}O_4$ is an inverse spinel with the Li^+ and three-fifths of the Fe^{3+} ions occupying the octahedral B sites of the cubic spinel structure of the general formula AB_2O_4 [8]. Moreover, lithium ferrite have been also promising substitutes for Ni–Cu–Zn ferrites in advanced planar ferrite devices, because of their low sintering temperature, high Curie temperature and excellent electromagnetic properties at high frequency [9]. Magnesium-substituted lithium ferrites have been used in many electronic devices for high frequency because of their high electrical resistivity, high Curie temperature and low cost [10]. In this study, we reported (1) the relationship between lattice constant between dopant content of Mg, in which the variation of lattice is related with the substitution sites of Mg^{2+}, (2) the relationship between the initial permeability with frequency, (3) determination of Curie temperature via the Arrhenius plots for electrical conductivity of Mg-substituted lithium ferrite, and (4) the microstructure dependence on the dopant content of Mg.

2. Experimental procedure

2.1. Preparation of magnesium-substituted lithium ferrites

Magnesium-substituted lithium ferrites $Li_{0.5}Fe_{2.5-x}Mg_xO_{4-\delta}$ with $0.0 \leq x \leq 1.0$ were prepared following the conventional ceramic method. Samples were prepared from reagent-grade powders of Li_2CO_3, MgO, and Fe_2O_3. Appropriate proportion of these compound were taken and ball-milled for 12 h in distilled

* Corresponding author. Tel.: +886 3 863 4209; fax: +886 3 863 4200.
E-mail address: d887503@alumni.nthu.edu.tw (Y.-P. Fu).

0272-8842/$36.00
doi:10.1016/j.ceramint.2009.12.019

water in order to mix them thoroughly and improved the homogeneity. The resulting mixtures were dried, and calcined at 700 °C for 4 h. Subsequently the whole mixture was remilled for 6 h and dried. The dried and sieved powder was pressed in the form of pellets using a small amount of PVA as binder with an applied unaxial pressure of 1000 kgf/cm^2. The pellets sample was then finally sintered at 1200 °C for 4 h in air and furnace cooled.

2.2. Characterization of the materials

Computerized X-ray powder diffraction (XRD; Rigaku D/Max-II, Tokyo, Japan) analysis, together with Cu Kα radiation with $\lambda = 0.15405$ nm was used to identify the crystalline phase and calculated lattice parameter. The morphological features of the magnesium-substituted lithium ferrites were carried out using a scanning electron microscope (SEM; Hitachi S-3500H, Tokyo, Japan). The electrical conductivity measurements were made at various temperatures in the range of 250–700 °C in air by the DC two probes technique. Pellet specimens (10 mm in diameter and 2 mm in thickness) were used for electrical conductivity measurement. Two Ag leads were attached on the sample with Ag paste and fired at 800 °C. Activation energy for conduction was obtained by plotting the ionic conductivity data in Arrhenius relation for thermally activated conduction. The initial permeability (μ_i) of magnesium-substituted lithium ferrite were measured on impedance analyzer (Agilent 4194A, Santa Clara, CA, USA) in the frequency range of 1 kHz to 100 MHz; 15 turns of coil were wound around the sintered toroidal specimens with dimension of 14 mm outer diameter, 7 mm inner diameter, and 3 mm thickness. All the measurements were carried out at room temperature.

3. Results and discussion

Unlike other spinel-type ferrites, lithium ferrite exists in two different crystalline forms. The α-phase has an FCC inverse spinel structure with space group of $P4_332$ and α-phase is an ordered phase in which the Li^+ and Fe^{3+} ions are ordered in the 1:3 ratio in the octahedral B sites of the cubic spinel structure, whereas the remaining Fe^{3+} ions occupy the tetrahedral A sites. Whereas the β-phase is a disordered phase where the Li^+ and Fe^{3+} ions are randomly distributed in the octahedral interstices and the space group is $Fd\bar{3}m$ [11–13]. Fig. 1 showed the X-ray diffraction patterns of the magnesium-substituted lithium ferrites specimens sintered at 1200 °C for 4 h. It was evident that the magnesium-substituted lithium ferrite specimens contain only the α-phase. All the peaks in the pattern were matched well with JCPDS card (No. 38-0259). No β-phase was detected in the XRD patterns of samples. The presence of α-phase is due to the fact that during the usual ceramic method of synthesis of the bulk ferrite, a slow cooling process form above 755 °C yields the ordered phase [11].

The introduction of Mg^{2+} ions into pure lithium ferrite can cause a small shift to a lower diffraction angle in the lithium

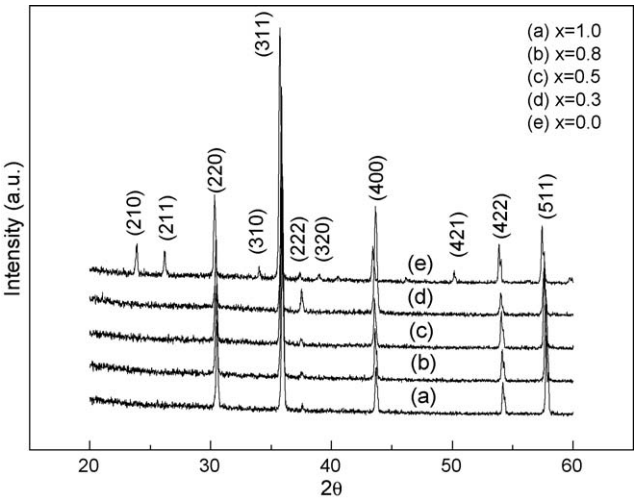

Fig. 1. X-ray powder pattern of magnesium-substituted lithium ferrites sintered at 1200 °C for 4 h.

ferrite peaks. This shift was indicative of the change in lattice parameter. Fig. 2 showed the dependence of the lattice constant on Mg-substituted content. The result revealed that the lattice constant increased gradually with increasing content of magnesium substitution in the range of $0.0 < x < 0.5$, and in the range of $0.5 < x < 1.0$, the lattice constant markedly increased as x increases. Generally, as the Mg-substituted content increase, the lattice constant increased. It was due to the fact that different radii of Fe^{3+} (0.64 Å), Mg^{2+} (0.71 Å), and Li^+ (0.76 Å) in an oxide solid solution with a spinel-type structure. When doped with larger size of Mg^{2+} ions in the spinel lithium ferrite, causing the spinel lithium ferrite swell. Doping Mg^{2+} ions in a spinel-type structure will induce uniform strain in the lattice as the material is elastically deformed [14]. This effect causes the lattice plane spacing to change and the diffraction peaks shift to a lower 2θ position. Noticeably, the lattice parameter was nonlinearly dependent on Mg-substituted concentration for $Li_{0.5}Fe_{2.5-x}Mg_xO_{4-\delta}$. We can define the chemical formulas of $(Fe_{1.0})$ $[Li_{0.5}Fe_{1.5}]O_4$ and $(Fe_{1.0-y}Li_y)$

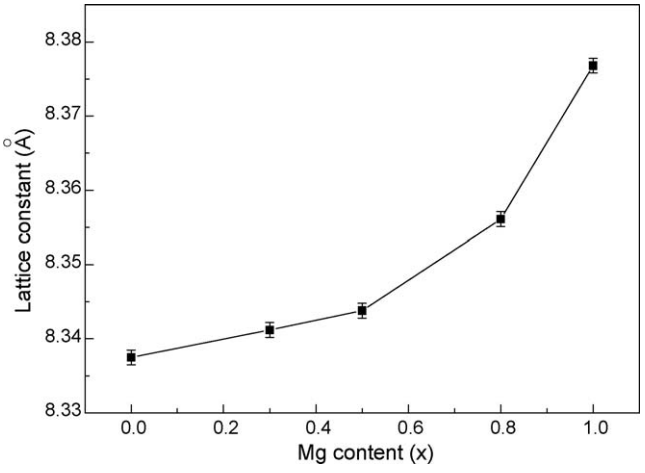

Fig. 2. Dependence of lattice constant vs dopant content of Mg.

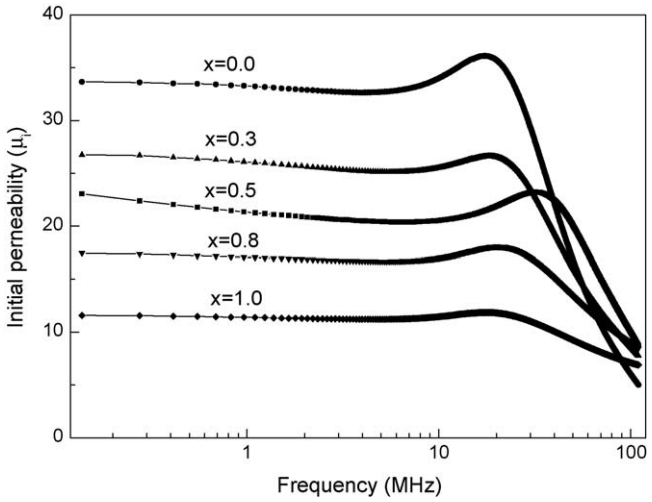

Fig. 3. Frequency dependence of permeability for magnesium-substituted lithium ferrite.

$[Li_{0.5-y}Fe_{1.5-x+y}Mg_x]O_4$ for $x = 0$ and $x > 0$, respectively. The formula for $x > 0$ indicates that Li^+ ions partially occupy the tetrahedral (A) site and that the distribution of Fe^{3+} ions occupying the tetrahedral (A) and octahedral [B] sites changes. y increases nonlinearly as x increases [15]. The observed nonlinear Mg-substituted content dependence of the lattice parameter may have resulted from the change of ion distribution depending on the content of Mg substitution.

It is well known that the initial permeability of ferrite is strongly affected by saturation magnetization, crystal magnetization anisotropy, magnetostriction constant, and internal stress. The initial permeability can be expressed as follows equation [16]: $\mu_i = (M_s^2/aK + b\lambda\sigma)$ where μ_i is the initial permeability, M_s is the saturation magnetization, K is the crystal magnetic anisotropy, λ is the magnetostriction constant, σ is the internal stress, a and b are constants. If in this equation, it is assumed that the crystal magnetization anisotropy, magnetostriction, and internal stress are constant, the saturation magnetization is predominant. The magnetic moment in ferrite is mainly due to the uncompensated electron spin of the individual ion and the spin alignments in the two sublattices which are arranged antiparallely. In a spinel ferrite, each ion at A site has 12 B-site ions as nearest neighbors. According to Neel's molecular field model [17], the AB super exchange interaction predominate the intrasublattice AA and BB interactions. Therefore, the net magnetic moment is given by the sum of the magnetic moments of A and B sublattices, i.e., $M = M_B - M_A$. In this study, the cationic distribution, Li^+ and Mg^{2+} are non-magnetic and do not contribute to the sublattice magnetization [18]. For magnesium-substituted lithium ferrite, Li^+ substitution for Fe^{3+} lions at A site, leading to a decrease in the A site sublattice magnetization. Moreover, the Fe^{3+} ions are replaced by non-magnetic Li^+ and Mg^{2+} ions, leading to a decrease in the B site sublattice magnetization. Therefore, the magnetization of both sublattices decreases. The decrease of the B site magnetization is stronger than one of A site, which leads to a fall in the net magnetization. With an increase of Mg^{2+} ions content in magnesium-substituted lithium ferrite, the net magnetization decreased gradually. Fig. 3 showed plot of the frequency dependence of initial permeability for sintered magnesium-substituted lithium ferrite specimens. In this study, it was found that the initial permeability was strongly influenced by the Mg-substituted content. This behavior is agrees well with the above-mentioned equation, which indicates that the initial permeability is predominant by magnetization. The initial permeability values of all specimens showed the flat profile from 0.1 to 10 MHz and then rise to a maximum before falling rapidly to low values due to ferromagnetic resonance. The dispersion of initial permeability at low frequency is attributed to domain wall displacement. For use in magnetic applications, the initial permeability should remain fairly constant over certain frequency ranges. For sintered pure lithium ferrite, the initial permeability of 34 showed a flat profile from 0.1 to 10 MHz and the maximum initial permeability of 40 was obtained at 24.6 MHz. Fig. 4 revealed the permeability as function of Mg-substituted concentration for $Li_{0.5}Fe_{2.5-x}Mg_xO_4$ specimens at 10 MHz. Obviously, the permeability reached the maximum value of $\mu(f = 10\ \text{MHz}) = 34.0$ for $Li_{0.5}Fe_{2.5}O_4$. However, further increasing Mg-substituted concentration, the permeability decreased gradually from $\mu(f = 10\ \text{MHz}) = 25.5$ for $x = 0.3$ to $\mu(f = 10\ \text{MHz}) = 11.5$ for the composition with $x = 1.0$, respectively. Because pure lithium ferrite specimen possesses the highest value of saturation magnetization among the magnesium-substituted lithium ferrite, pure lithium ferrite specimen has the highest value of initial permeability. With an increase of Mg-substituted content, the saturation magnetization value decreased gradually. This will lead to the values of permeability decrease with increasing Mg-substituted content.

In general, the conductivity of spinel ferrites is due to the presence of Fe^{2+} ions. The conductivity arises due to the mobility of the extra electron, which comes from Fe^{2+} through the crystal lattice. The movement is described by a hopping mechanism, in which the charge carries jump from one ionic site to the next [19]. The cation distributions of lithium ferrite

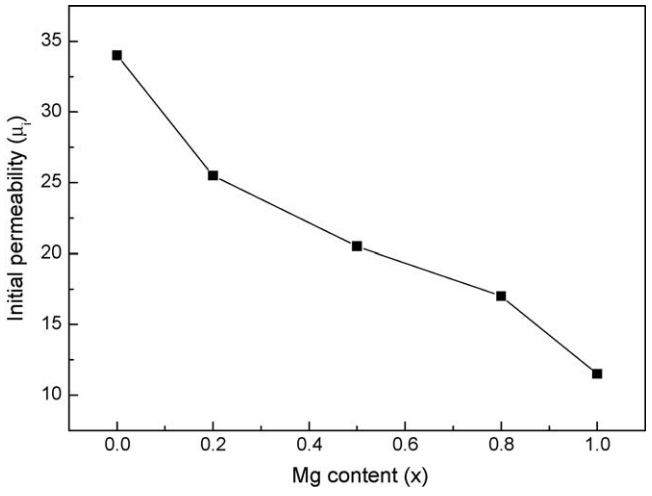

Fig. 4. Initial permeability of $Li_{0.5}Fe_{2.5-x}Mg_xO_{4-\delta}$ specimens.

Table 1
Electrical conductivity the $Li_{0.5}Fe_{2.5-x}Mg_xO_{4-\delta}$ system in the temperature range of 550–700 °C.

Materials	Conductivity (S/cm)		
	600 °C	650 °C	700 °C
$x = 0.0$	1.10×10^{-1}	1.22×10^{-1}	1.27×10^{-1}
$x = 0.3$	2.08×10^{-2}	2.99×10^{-2}	4.08×10^{-2}
$x = 0.5$	2.54×10^{-3}	4.50×10^{-3}	7.79×10^{-3}
$x = 0.8$	7.67×10^{-4}	1.63×10^{-3}	3.42×10^{-3}
$x = 1.0$	1.14×10^{-4}	4.08×10^{-4}	1.35×10^{-3}

and magnesium-substituted lithium ferrite having the inverse spinel structure are given by $(Fe^{3+}_{1.0})[Li^{+}_{0.5}Fe^{3+}_{1.5}]O^{2-}_4$ and $(Fe^{3+}_{1.0-y}Li^{+}_{y})[Li^{+}_{0.5-y}Fe^{3+}_{1.5-x+y}Mg^{2+}_{x}]O^{2-}_4$ for $x = 0$ and $x > 0$, respectively, where the parentheses denote tetrahedral sites (A sites) and square brackets denote octahedral sites (B site). The formula for $x > 0$ indicates that Li^+ ions partially occupy the tetrahedral (A) site and that the distribution of Fe^{3+} ions occupying the tetrahedral (A) and octahedral (B) sites changes. For lithium ferrite, the conduction by hoping mechanism taking place between Fe^{2+} and Fe^{3+} ions present on equivalent crystallographic sites in the structure of the ferrite is given as follow [20]: $Fe^{2+} \Leftrightarrow Fe^{3+} + e^-$ In this model, the electron transfer between adjacent octahedral sites in spinel lattice. Local displacement of electrons in the direction of applied electric field can be obtained that occur due to the displacement in determining the polarization of ferrite [21]. However, in lithium ferrite, there are no Fe^{2+} ions. The existence of Fe^{2+} is due to the fact that the preparation of ferrite requires high temperature sintering at 1150–1250 °C for obtaining dense material, at these temperature oxygen dissociation and lithia volatility, the consequence is reduction of Fe^{3+} ions Fe^{2+} ions. The temperature dependence of the electrical conductivity for all specimens was shown in Fig. 5. The maximum electrical conductivity, $\sigma_{700\ ^\circ C} = 0.1274$ S/cm was found for $Li_{0.5}Fe_{2.5}O_4$ specimen. Table 1 summarized the

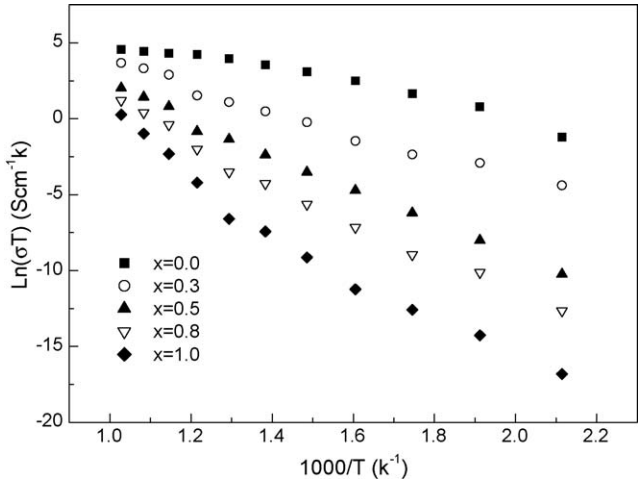

Fig. 5. Arrhenius plots for electrical conductivities of magnesium-substituted lithium ferrite.

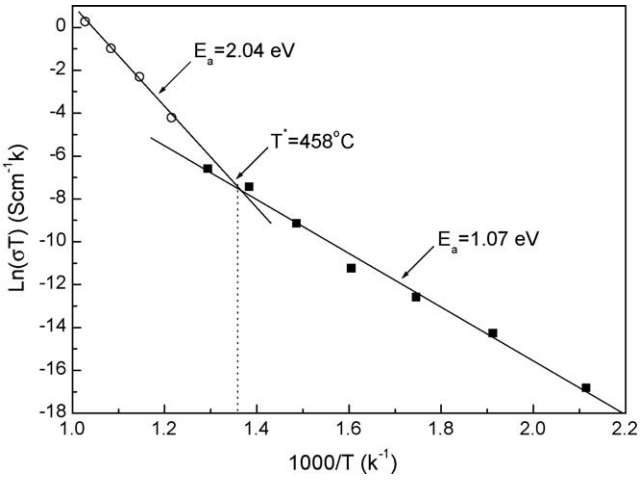

Fig. 6. Temperature dependence of electronic conductivity of magnesium-substituted lithium ferrite.

electrical conductivity as a function of Mg-substituted content for magnesium-substituted lithium ferrite in the temperature range of 550–700 °C. The experimental results revealed that the electrical conductivity decreases with increasing the Mg-substituted content in the temperature range of 250–700 °C. This phenomenon can be explained as the Mg^{2+} ions substituted for Fe^{3+} ions, resulting in the decrease for Fe^{3+} content. Due to the high temperature sintering, Fe^{3+} ions is partially reduced to Fe^{2+} ions in lithium ferrite. The content of Fe^{2+} ions is decreased with increasing the Mg^{2+} ions substituted for Fe^{3+} ions. With increasing the Mg-substituted content, the electrical conductivity is decreased. The Mg^{2+} substituted for Fe^{3+} may restrain the content of Fe^{2+} in lithium ferrite.

The small activation energy value for the electron conduction and the linear relation between $\log \sigma T$ vs $(1/T)$ might indicate that the small polaron model of electron hopping motion between Fe^{2+} and Fe^{3+} offer the best possibility for charge transfer mechanism for pure lithium ferrite [22]. A small polaron is a defect created when an electron carrier becomes trapped at a given site as a consequence of the displacement of adjacent ions. The entire defect then migrates by an activated hopping mechanism. Small polaron formation can take place in materials whose conduction electron belong to incomplete inner (d or f) shells which due to small electron overlap, tend to form extremely narrow bands. The possibility for the occurrence of hopping conductivity in certain low mobility semiconductor, especially oxides has been widely recognized for some time. According the previous literatures [23], we can conclude that because lithium ferrite is a low mobility conductor, it obeys the small polaron model.

As shown in Fig. 6, an Arrhenius plot of $Li_{0.5}Fe_{1.5}Mg_{1.0}O_{3.75}$ specimen would give two straight lines intersecting at $T^* = 458$ °C. The conductivity variation showed two different regions with a large variation in the activation energy. This behavior was similar to that known in the case of similar ferrite with a transformation in the slope of Arrhenius plot at a certain temperature. Similar behaviors were also observed in all

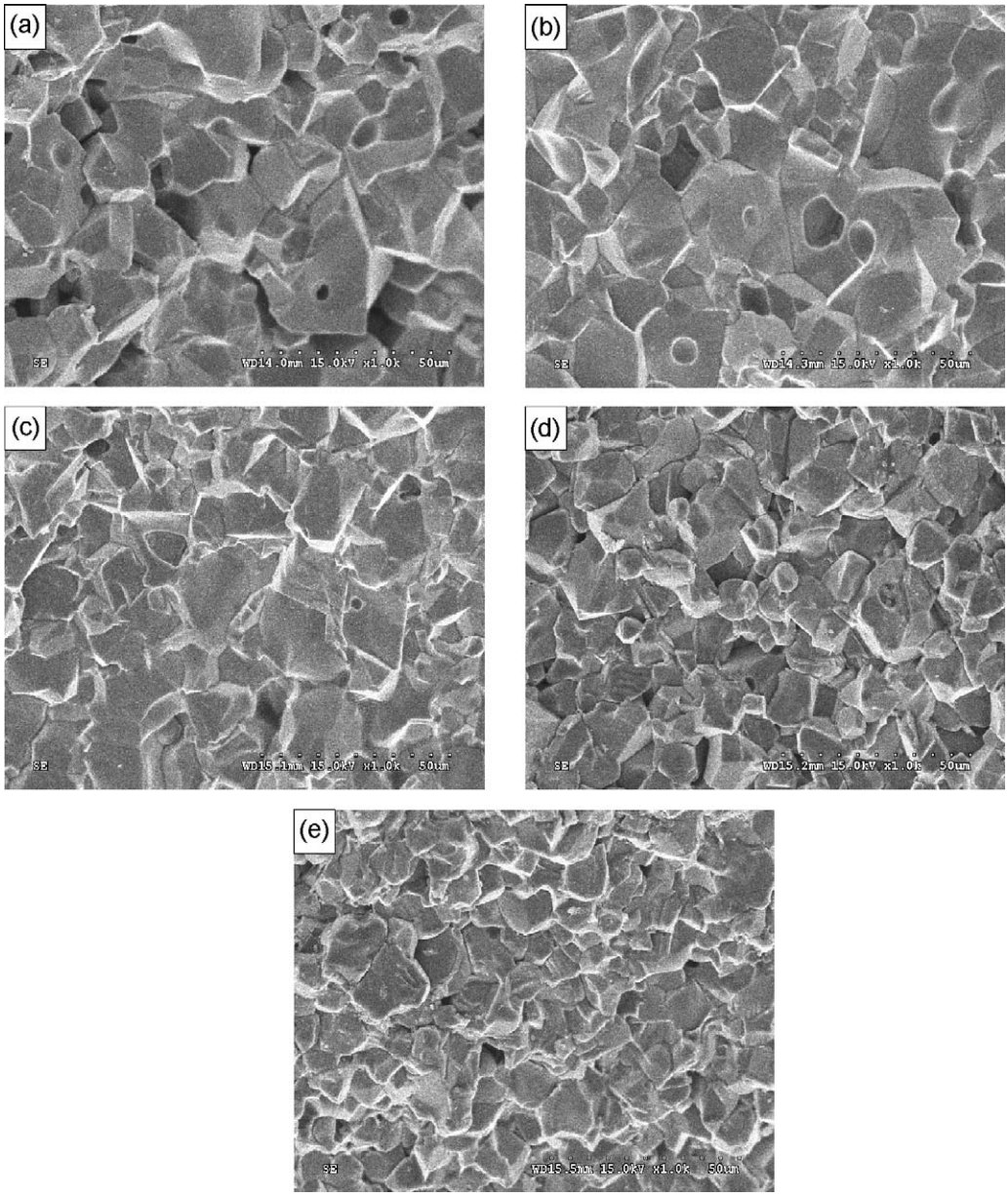

Fig. 7. Typical fracture microstructure of $Li_{0.5}Fe_{2.5-x}Mg_xO_{4-\delta}$ specimens for (a) $x = 0.0$, (b) $x = 0.3$, (c) $x = 0.5$, (d) $x = 0.8$, and (e) $x = 1.0$.

magnesium-substituted lithium ferrite specimens. The two straight lines given a linear fit of these equations to the data measured with the follow regressed equations:

For $Li_{0.5}Fe_{2.5}O_4$ ($T^* = 591$ °C):

$$\ln(\sigma T) = (13.812) - (7.835)\frac{1000}{T}(T < T^*)$$

$$\ln(\sigma T) = (8.224) - (3.259)\frac{1000}{T}(T > T^*)$$

For $Li_{0.5}Fe_{2.2}Mg_{0.3}O_{3.85}$ ($T^* = 567$ °C):

$$\ln(\sigma T) = (9.560) - (8.023)\frac{1000}{T}(T < T^*)$$

$$\ln(\sigma T) = (15.324) - (11.150)\frac{1000}{T}(T > T^*)$$

Table 2
Transition temperature and activation energy of the $Li_{0.5}Fe_{2.5-x}Mg_xO_{4-\delta}$ system.

Materials	Transition temperature (T^*) in °C	Activation energy, Ea (eV)	
		Below T^*	Above T^*
$x = 0.0$	591	0.28	0.61
$x = 0.3$	567	0.95	0.69
$x = 0.5$	550	1.27	0.92
$x = 0.8$	476	1.44	0.96
$x = 1.0$	458	2.04	1.07

For $Li_{0.5}Fe_{2.0}Mg_{0.5}O_{3.75}$ (T^* = 550 °C):

$$\ln(\sigma T) = (12.508) - (10.745)\frac{1000}{T}(T < T^*)$$

$$\ln(\sigma T) = (17.483) - (14.873)\frac{1000}{T}(T > T^*)$$

For $Li_{0.5}Fe_{1.7}Mg_{0.8}O_{3.60}$ (T^* = 476 °C):

$$\ln(\sigma T) = (13.002) - (12.597)\frac{1000}{T}(T < T^*)$$

$$\ln(\sigma T) = (18.605) - (16.819)\frac{1000}{T}(T > T^*)$$

For $Li_{0.5}Fe_{1.5}Mg_{1.0}O_{3.50}$ (T^* = 458 °C):

$$\ln(\sigma T) = (9.527) - (12.543)\frac{1000}{T}(T < T^*)$$

$$\ln(\sigma T) = (24.723) - (23.730)\frac{1000}{T}(T > T^*)$$

The activation energy calculated from the two different region in the Arrhenius plot were listed in Table 2 along with the transition temperature (T^*). So far the theory about conductivity mechanism for lithium ferrite can be divided into two types. Manjula et al. [24] reported that the transformation in slope may be due to the change in the conduction mechanism. For $T < T^*$ region, the conduction mechanism may be due to electron hopping between Fe^{2+} and Fe^{3+} in the octahedral sites. For $T > T^*$ region, the mechanism is probably due to ionic conduction caused by lithium ions in the octahedral sites. However, Ravinder et al. [25] propose that a change of slope in the Arrhenius plot may be due to the ferri to paramagnetic transition from low to high temperature. According to the experimental results, it was found that the transition temperature was close to the Curie temperature. Therefore, the change in slope in Arrhenius plots for electrical conductivities may be due to the magnetic transition. In this study, the transition temperature (T^*) represented the Curie temperature (T_C). Similar transitions in a neighborhood of Curie temperature have also been observed by several investigators in various ferrite systems [26–28]. Moreover, it was found that the electrical conductivity was measured only up to 277 °C for Manjula's experiment results. The Curie temperature of lithium ferrite was much higher than his measurement temperature. If he increased the measured temperature for electrical conductivity, he may probably observe the magnetic transition in transition temperature. In the ferromagnetic region, the activation energies of all the samples were in the range from 0.28 to 2.04 eV. However, for paramagnetic region, the activation energies of all the samples were in the range from 0.61 to 1.07 eV. Generally, the activation energies in the ferromagnetic region were greater than those in the paramagnetic region. The microstructure will significantly influence the dielectric and magnetic properties for magnesium-substituted lithium ferrite. Fig. 7 illustrated the microstructure of magnesium-substituted lithium ferrite specimens, indicating that the grain size significantly depended on the Mg-substituted content. The result revealed that the average grain size of magnesium-substituted lithium ferrite decreased gradually with increasing Mg-substituted content. This indicated that addition with the magnesium in lithium ferrite inhibited the grain growth and fined the grain size.

4. Conclusions

The effect of Mg-substituted content on magnetic and electronic properties for magnesium-substituted lithium ferrites had been systematically studied in this paper. The permeability decreased gradually from μ (f = 10 MHz) = 34.0 for $Li_{0.5}Fe_{2.5}O_4$ to μ (f = 10 MHz) = 11.5 for $Li_{0.5}Fe_{1.5}Mg_{1.0}O_4$. The variation of electrical conductivity with temperature can be explained using the small hopping mechanism. The maximum electrical conductivity, $\sigma_{700\ °C}$ = 0.1274 S/cm was found to be for $Li_{0.5}Fe_{2.5}O_4$ specimen. With an increase of Mg-substituted content, the electrical conductivity was decreased. A change of slope in the Arrhenius plot may be due to the magnetic transition.

References

[1] S.C. Watawe, U.A. Bamne, S.P. Gonbare, R.B. Tangsali, Preparation and dielectric properties of cadmium substituted lithium ferrite using microwave-induced combustion, Mater. Chem. Phys. 103 (2007) 323–328.
[2] X. Qi, J. Zhou, Z. Yue, Z. Gui, L. Li, Permeability and microstructure of manganese modified lithium ferrite prepared by sol–gel auto-combustion method, Mater. Sci. Eng. B 99 (2003) 278–281.
[3] H.M. Widatallah, C. Johnson, F. Berry, M. Pekala, Synthesis, structural, and magnetic characterisation of magnesium-doped lithium ferrite of composition $Li_{0.5}Fe_{2.5}O_4$, Solid State Commun. 120 (2001) 171–175.
[4] G.M Argentina, P.D. Baba, Microwave lithium ferrite: an overview, IEEE Trans. Microwave Theory Technol. 22 (1974) 652–658.
[5] J.S. Baijal, S. Phanjoubam, D. Kothari, C. Prakash, P. Kishan, Hyperfine interactions and magnetic studies of Li–Mg ferrites, Solid State Commun. 83 (1992) 679–682.
[6] Y.P. Fu, C.S. Hsu, $Li_{0.5}Fe_{2.5-x}Mn_xO_4$ ferrite sintered from microwave-induced combustion, Solid State Commun. 134 (2005) 201–206.
[7] Y.P. Fu, Microwave-induced combustion synthesis of $Li_{0.5}Fe_{2.5-x}Cr_xO_4$ powder and their characterization, Mater. Res. Bull. 41 (2006) 809–816.
[8] S. Verma, P.A. Joy, Magnetic properties of superparamagnetic lithium ferrite nanoparticles, J. Appl. Phys. 98 (2005) 124312.
[9] Z. Yue, J. Zhou, X. Wang, Z. Gui, L. Li, Preparation and magnetic properties of titanium-substituted LiZn ferrites via a sol–gel auto-combustion process, J. Eur. Ceram. Soc. 23 (2003) 189–193.
[10] D. Ravinder, P.V.B. Reddy, Thermoelectric power studies of polycrystalline magnesium substituted lithium ferrites, J. Magn. Magn. Mater. 263 (2003) 127–133.
[11] S. Verma, J. Karande, A. Patidar, P.A. Joy, Low-temperature synthesis of nanocrystalline powders of lithium ferrite by an autocombustion method using citric acid and glycine, Mater. Lett. 59 (2005) 2630–2633.
[12] A. Tomas, P. Laruelle, J.L. Dormann, M. Nogues, Affinement de la structure des formes ordonnée et désordonnée de l'octaoxopentaferrate de lithium, $LiFe_5O_8$, Acta Crystallogr. C 39 (1983) 1615–1617.
[13] S.J. Marin, K. O'Keefe, D.E. Partin, Structures and crystal chemistry of ordered spinels: $LiFe_5O_8$, $LiZnNbO_4$, and Zn_2TiO_4, J. Solid State Chem. 113 (1994) 413–419.
[14] Y.P. Fu, C.H. Lin, Microwave-induced combustion synthesis of $Li_{0.5}Fe_{2.5-x}Mg_xO_4$ powder and their characterization, J. Appl. Phys. 105 (2009) 07A505.
[15] E.W. Gorter, Saturation magnetization and crystal chemistry of ferrimagnetic oxides. I. II. Theory of ferrimagnetism, Philips Res. Rep. 9 (1954) 295–320.
[16] M. Fjimotou, K. Hoshi, M. Nakazawa, S. Sekiguchi, Cu multiply twinned particle precipitation in low-temperature fired Ni–Zn–Cu ferrite, Jpn. J. Appl. Phys. Part 1 32 (1993) 5532–5536.

[17] B.D. Cullity, Introduction to Magnetic Materials, Addison-Wesley, MA, 1972,, p. 141.
[18] M. Maisnam, S. Phanjoubam, H.N.K. Sarma, C. Prakash, L.R. Devi, O.P. Thakur, Magnetic properties of vanadium-substituted lithium zinc titanium ferrite, Mater. Lett. 58 (2004) 2412–2414.
[19] B. Viswanathan, V.R.K. Murthy, Ferrite Materials Science and Technology, Norosa Publishing House, New Delhi, 1990, p. 38.
[20] V.R.K. Murthy, S. Sundaram, B. Viswanathan, Microwave Materials, Springer-Verlag, New York, 1994, p. 143.
[21] R.K. Kotnala, V. Verma, V. Pandey, V.P.S. Awana, P.P. Aloysius, P.C. Kothari, The effect of nano-SiO_2 on the magnetic and dielectric properties of lithium cadmium ferrite, Solid State Commun. 143 (2007) 527–531.
[22] H.L. Tuller, A.S. Nowick, Small polaron electron transport in reduced CeO_2 single crystals, J. Phys. Chem. Solids 38 (1977) 859–867.
[23] I.G. Austin, N.F. Mott, Polarons in crystalline and non-crystalline materials, Adv. Phys. 18 (1969) 41–102.
[24] R. Manjula, V.R.K. Murthy, J. Sobhanadri, Electrical conductivity and thermoelectric power measurements of some lithium–titanium ferrites, J. Appl. Phys. 59 (1986) 2929–2931.
[25] D. Ravinder, G. Ranga Mohan, D.R. Sagar, Prankishan, N. Kumar, Electrical conductivity and thermoelectric power studies of aluminium-substituted lithium ferrites, Mater. Lett. 43 (2000) 122–128.
[26] M. Pal, P. Brahma, D. Chakravorty, Magnetic and electrical properties of nickel–zinc ferrites doped with bismuth oxide, J. Magn. Magn. Mater. 152 (1996) 370–374.
[27] M.A. El Hiti, DC conductivity for $Zn_xMg_{0.8-x}Ni_{0.2}Fe_2O_4$ ferrites, J. Magn. Magn. Mater. 136 (1994) 138–142.
[28] D. Ravinder, T. Seshagiri Rao, Electrical conductivity and thermoelectric power of lithium–cadmium ferrites, Cryst. Res. Technol. 25 (1990) 963–969.